



AIAA 2002-0905

Measurement and Numerical Prediction of  
Homogeneous Turbulent Flow over a Cylinder:  
A Baseline for Droplet-Laden Flow Studies

C. Presser, and J.F. Widmann  
National Institute of Standards and Technology  
Gaithersburg, MD 20899-8360

P.E. DesJardin, and L.A. Gritzo  
Sandia National Laboratory  
Albuquerque, NM 87185-0836

**40th AIAA Aerospace Sciences  
Meeting & Exhibit  
14-17 January 2002 / Reno, NV**



## MEASUREMENT AND NUMERICAL PREDICTION OF HOMOGENEOUS TURBULENT FLOW OVER A CYLINDER: A BASELINE FOR DROPLET-LADEN FLOW STUDIES

Cary Presser<sup>\*</sup>, and John F. Widmann<sup>†</sup>  
National Institute of Standards and Technology  
100 Bureau Drive, Stop 8360  
Gaithersburg, MD 20899-8360 USA

Paul E. DesJardin<sup>‡</sup>, and Louis A. Gritzo<sup>§</sup>  
Sandia National Laboratories  
P.O. Box 5800  
Albuquerque, NM 87185-0836 USA

### Abstract

The focus of this effort is to investigate the dispersal of liquid fire suppression agents around solid obstacles, and obtain a better understanding of the physical processes of droplet transport in cluttered spaces. A combined experimental/numerical study is presented to examine the flow field dynamics of highly turbulent flow over obstacles, and spray transport in such flow fields. Comparison of numerical predictions to particle image velocimetry (PIV) measurements shows good qualitative agreement in spatial distribution of the mean and RMS velocities with a 20 % overprediction in mean streamwise velocity and 15 % underprediction in RMS. These results provide a baseline for future spray experiments. A numerical sensitivity study using HFE-7100 agent reveals a strong dependency of droplet penetration on initial droplet size for the flow range and droplet sizes that are of interest in practical agent delivery systems.

### Introduction

The new generation of Halon replacements include chemical fire suppressants that have high boiling point temperatures (*i.e.*,  $T_b > 330$  K) and exist in liquid phase under high-pressure release or in

ambient conditions. Release of these agents in a confined space results in the dispersal of droplets that will either travel along ballistic trajectories, move with the convecting flow, or a combination of the two depending on the local Stokes number of the droplet. Therefore, accurate representation of droplet transport is crucial for numerical modeling of fire suppression in confined spaces using these agents.

To better understand the physics of droplet dispersion around solid objects, an experimental arrangement at the NIST spray facility was modified to impose controlled grid-generated turbulence on the air stream. Experimental results from this facility will provide new experimental data for a well-characterized, homogenous droplet-laden turbulent flow field around a prescribed obstacle. Baseline measurements of the single gas-phase velocities with and without obstacles, but without the spray, are reported in this study. Operating conditions were based on typical engine nacelle-like conditions to study atomization and dispersion of a liquid agent around three cylinders that were chosen as representative obstacles. The cylinder diameters were smaller than, similar to, and larger than the characteristic length scale of turbulence to explore the effects of turbulence intensity on clutter size. In addition to the experiments, numerical simulations using the

<sup>\*</sup> Group Leader, Chemical Science and Technology Laboratory, Associate Fellow AIAA, corresponding author, e-mail: cpresser@nist.gov

<sup>†</sup> Chemical Engineer, Building and Fire Research Laboratory, member AIAA

<sup>‡</sup> Senior Member of Technical Staff, Fire Science and Technology Department, member AIAA

<sup>§</sup> Manager, Fire Science and Technology Department

This material is declared a work of the U.S. Government and is not subject to copyright protection in the United States.

VULCAN Computational Fluid Dynamics (CFD) fire physics code were conducted and the predictions compared to the experimental measurements of gas mean velocity and turbulent fluctuations. A sensitivity study is also conducted as part of the CFD calculations to explore the dispersal of liquid droplets around the obstacles as a function of initial droplet size. The motivation of this exercise is to understand the droplet transport processes that govern agent transport to regions behind solid objects.

This paper presents a description of the experimental arrangement, diagnostics that were used to characterize the flow field, and the CFD model. The results from both the experimental measurements and numerical simulations are compared and discussed, along with comments on future work.

### Experimental Arrangement

In order to explore droplet transport around obstacles, an experimental arrangement is used that provides a well-characterized, homogeneous turbulent flow field around prescribed obstacles, and is shown in Figs. 1 and 2. The experimental facility includes an air swirl burner that is used in the reported experiments to provide nonswirling air to the experiment, and coflows around the liquid agent injector. Additional details on the design of the burner are available elsewhere [1]. An octagon-shaped Plexiglas insert (with a wall thickness of 6 mm, length of 610 mm, and major and minor axes of 760 mm and 560 mm) was used as a boundary condition (generically shown in Fig. 1). A honeycomb layer (51 mm thick with 3 mm size cells) is used to straighten the airflow, which is co-positioned around an injector for the agent. Grid-generated turbulence on the air stream is imposed by placing a layer of wire mesh screen (with 13 mm size cells) downstream of the honeycomb. For these experiments, the incoming air (supplied from a 7 L/min compressor) was directed entirely through a selected 125 mm by 254 mm rectangular cross sectional portion of the honeycomb and then through wire mesh screen (placed 25 mm downstream of the honeycomb), as shown in Fig. 2. The integral and Kolmogorov length scales of turbulence are estimated to be 3 cm and 100  $\mu\text{m}$ , respectively. Three cylinders with diameters of 3 mm, 13 mm, and 32 mm, were chosen to span ranges of clutter sizes smaller than, on the same order of, and larger than the integral length scales of turbulence. The obstacles were placed 100 mm downstream of the honeycomb. Choice of

location of the screen and obstacles is discussed further in the next section. A stepper-motor-driven traversing system translates the entire assembly, and permits measurements of the flow field properties at selected locations downstream of the injector.

The mean gas velocities were initially estimated with a five-hole pitot probe and two-component phase Doppler interferometer. Although the overall results (as opposed to the detailed measurement profiles) are mentioned later in the text, a brief description of these two diagnostics is given here for completeness. The five-hole pitot probe has a hemispherical head that is 1.7 mm in diameter. The head is attached to a cylindrical body for a length of 26 mm, and then the diameter of the probe increases smoothly from 1.7 mm to 3.2 mm, which is the diameter of the main body of the probe. The probe has one hole on the head of the probe tip for total pressure measurements, and four holes located 13 mm from the head and 90° apart on the side of the probe for static pressure measurements.

The average of the four velocity measurements is reported as the mean velocity. Mean gas velocities were also obtained at selected points by seeding the air flow field with 1  $\mu\text{m}$  particles, generated with a pencil fogger, and using a two-component phase Doppler interferometer (PDI) from TSI, Inc.\* This system will be used more extensively in the next phase of this work (not reported here), in which liquid agent will be introduced to the flow field, to obtain spatial profiles of the droplet size and velocity distributions, and droplet number density. The receiving optics were aligned at a 25° scattering angle measured from the forward direction of propagation of the laser beams, and the transmitting and receiving optics were aligned at the same elevation. A 5 W argon ion laser operating in multi-line mode was used as the illumination source. The blue (wavelength = 488 nm) and green (wavelength = 514.5 nm) lines of the argon ion laser are separated and focused by the transmitting optics to intersect and form the probe volume.

---

\* Certain commercial equipment or materials are identified in this publication to specify adequately the experimental procedure. Such identification does not imply recommendation or endorsement by the National Institute of Standards and Technology, nor does it imply that the materials or equipment are necessarily the best available for this purpose.

Table 1: HFE-7100 Thermodynamic Properties.

Property	Value
Molecular Weight	250 g/mol
Boiling Temperature	334 K
Critical Temperature	468.3 K
Heat of Vaporization @ B.P.	111.6 kJ/kg
Specific Heat @ room temperature	1183 J/kg
Density @ room temperature	1520 kg/m <sup>3</sup>

The flow field was characterized using a three-dimensional particle image velocimetry (PIV) system from Dantec Dynamics, Inc. PIV is a non-intrusive field measuring technique (as opposed to a single-point diagnostic method) that can measure two or three components of velocity. The method requires seed particles to be added to the flow, which are then assumed to follow the streamlines and act as tracers. The spatial displacement of the seed particles corresponding to two images separated by a known time period is measured, and the velocity is deduced. The pencil fogger generates seed particles approximately 1  $\mu\text{m}$  in diameter. The images are obtained in a plane corresponding to the laser light sheet, and the time between the images is determined by the time between laser pulses. The spatial resolution of the measurements depends directly upon the pixel resolution, field of view, and laser light sheet thickness, and indirectly on the seeding density. For the measurements presented here, the spatial resolution was approximately 600  $\mu\text{m}$ . The 3-D stereo PIV system differs from traditional PIV systems in that two CCD cameras are used, and three velocity components are measured [2].

A 50 mJ Nd:YAG laser was used as the illumination source for the PIV measurements. The pulse duration of the laser light sheet was about 5 ns, and the wavelength of the light was 532 nm. A pair of 12-bit double-frame CCD cameras with a resolution of 1024 x 1280 pixels was used to obtain the images. Special camera mounts were utilized to permit the rotation of the camera body with respect to the camera lens so the Scheimpflug condition was satisfied, permitting the laser sheet to be in focus despite the non-orthogonal camera alignment [2]. Bandpass filters (center wavelength = 532 nm, acceptance window = 30 nm) were used to reject the broadband white light from the room. The two cameras were placed at angles of about 70° and 110°, as measured from the forward direction of propagation of the laser pulse. The processed results are presented as a composite mapping of

individual planar regions that are about 40 mm in height and 50 mm in width. Statistics were obtained from about 500 - 700 individual records. Each field of view represents about 9000 vectors. Measurements of the flow field were carried out along the central plane of the measurement area, and at two planes,  $\pm 25$  mm from the central location.

#### CFD Spray Modeling

As a complement to the experimental measurements, a general-purpose fire simulation code, VULCAN, was used to conduct a parametric study of spray transport around the largest of the cylinders considered in the experiment. Specific details on numerical methods and modeling used in VULCAN, as well as the spray model, can be found in Ref. [3]. A 3D mesh was generated for the entire experimental facility with a total grid size of 26 x 51 x 80 = 106,080 cells. The initial conditions of the calculation are chosen to best match the experiment by setting the mean streamwise velocity, turbulence kinetic energy and its dissipation to values of 4.5 m/s, 0.304 m<sup>2</sup>/s<sup>2</sup> and 0.0212 m<sup>2</sup>/s<sup>3</sup>, respectively. The agent considered in this parameter study is HFE-7100 (C<sub>4</sub>F<sub>9</sub>OCH<sub>3</sub>), see Ref. [4]. Many of the thermodynamic parameters of HFE-7100 that are needed for input to the spray model, are available from the manufacturer, and summarized in Table 1. However, the gas-phase enthalpy of HFE-7100 is not readily obtainable and so only one-way coupling of the gas phase onto the spray transport is explored in this study. Future studies will consider two-way coupling effects.

#### Results And Discussion

Preliminary characterization of the flow field uniformity was determined by means of planar Mie scattering flow visualization, pitot probe, and a two-component phase Doppler interferometer for different airflow speeds. The results indicated a flow mean velocity of 4.5 m/s, corresponding to a

Reynolds number of 3700 (based on the grid cell size), and provide a homogenous distribution of turbulence across the measurement area. This flow velocity is also representative of airflow speeds through aircraft engine nacelles.

Particle image velocimetry (PIV) was used to obtain instantaneous two-dimensional images of the air flow field velocity (*i.e.*, three components of velocity). These images were then used to construct profiles of the air velocity characteristics, both upstream and downstream of the cylinder, and along the central plane of the aforementioned honeycomb rectangular cross sectional area. The characteristics presented are the streamwise ( $W$ ) and two cross-stream ( $U$  and  $V$ ) mean velocities (see Fig. 3), turbulence intensity ( $T_i$ , where  $i = U, V, W$ , see Fig. 4), and correlation coefficients of the turbulent velocity fluctuations ( $\rho$ , from which the Reynolds stresses can be derived, see Fig. 5). Downstream of the honeycomb, the baseline flow field was found to be relatively uniform throughout the measurement field, as shown in Figs. 3 and 4 (maximum gas streamwise component of velocity,  $W \cong 4.5$  m/s, and maximum turbulence intensity,  $T_w \cong 13$  %), except immediately downstream of the honeycomb. (Note the change in ordinate scales in Fig. 3.) The local jetting downstream of the honeycomb exit decays with increasing streamwise distance, and becomes negligible after 25 mm. Based on this observation, the wire grid mesh that is used to generate turbulence was placed at this location.

The flow downstream of the wire mesh was obtained along the central plane of the measurement region. Nonuniformities of the flow, due to the presence of the mesh, were created downstream of the mesh and relaxed to roughly a homogeneous state of 9 % turbulence intensity in each direction at 100 mm downstream of the honeycomb ( $W \cong 4.0$  m/s). The obstacles were placed at this location, shown with black circles, to study the effects of the turbulence, and eventually spray transport, around the cylinders in this well-controlled turbulent environment. The free stream air velocity remains at  $W \cong 5.0$  m/s around the side of the cylinders, and the flow behind each cylinder forms a recirculation region ( $W \cong -1.0$  m/s). The reverse flow behind the cylinders appears to extend about two cylinder diameters downstream. The turbulence intensity increases behind the cylinders ( $T_w \cong 20$  % in a banded region behind the obstacle). There is a significant correlation of the velocity fluctuations downstream of the cylinder between

the streamwise and  $V$ -cross-stream components (an absolute value of 0.7 is reached for the correlation coefficient, see Fig. 5). This result is indication of the shear between the free stream and recirculation region behind the cylinder. The flow also decelerates to a stagnation region at the centerline, at the upstream face of the cylinders. The overall flow characteristics around each cylinder appear to be similar, except that the features grow proportional to the cylinder diameter.

Comparisons of the CFD predictions of Figs. 6 and 7 to the PIV measurements indicate that qualitatively the location and size of the recirculation zone for the largest cylinder case is well captured. A two-dimensional slice of the mesh is presented in Fig. 6(a), and shows local grid refinement in regions near the cylinder to properly resolve the shear layer.

Quantitative comparison indicates that the numerical results over-predict the streamwise mean velocity by 20 % and under-predict the root mean square values in streamwise velocity by 15 %. These differences indicate that the numerical predictions under estimate the extent of turbulent mixing behind the cylinder, and may be attributed to the use of the  $k-\epsilon$  model that is known to perform poorly in highly recirculating flows.

Successive experimental work is to inject a liquid fire suppressant agent and to study the change in droplet transport as the spray interacts with the obstacles. One possible choice is HFE-7100 (boiling point of 334 K) since it has been shown to be effective at extracting heat from a flame zone [4]. Preliminary modeling results of this arrangement are presented in Figs. 8 and 9. The spray is modeled as a stream of droplets with a mass load rate of 1.598 g/s and zero slip for the droplets (*i.e.*, a droplet streamwise velocity of 4.5 m/s). Figures 8 and 9 present instantaneous snapshots of the spray distribution and velocity for three assumed initial droplet sizes of 10  $\mu\text{m}$ , 50  $\mu\text{m}$ , and 100  $\mu\text{m}$ . These droplet sizes are chosen to span the range of credible scenarios during agent release, and illustrate some interesting behavior. Note that the droplets are represented in the figures by a symbol of constant size, however, droplet vaporization does decrease the droplet size after injection into the computational domain. Figures 8(a) and 8(b) present results for the extreme 10  $\mu\text{m}$  and 100  $\mu\text{m}$  droplet cases. In both cases, droplet transport is not achieved beyond the cylinder because they are either too small and evaporate

before reaching the cylinder (*i.e.*, the 10  $\mu\text{m}$  case) or too large and follow a ballistic trajectory that results in direct impact into the cylinder (*i.e.*, the 100  $\mu\text{m}$  case). However, for the 50  $\mu\text{m}$  case considerable droplet transport is achieved beyond the cylinder, as shown in Fig. 9. In this case, the droplets are large enough not to evaporate too quickly, yet small enough to follow the streamlines and accelerate around the cylinder. Future efforts will focus on exploring this scenario experimentally, and investigating other realistic liquid agent release conditions.

#### Next Phase

This experimental work will study droplet transport processes of liquid fire suppressant agent in the regions upstream and downstream of different obstacle configurations. The experimental arrangement will be oriented horizontally, in order to estimate the ratio of liquid agent that impinges on the obstacle and the amount of agent transported past the obstacle. The grid-generated turbulence field will be altered by the presence of the liquid spray. The liquids that will be used are water and HFE-7100 (boiling point of 334 K) because of the effectiveness of high boiling point liquids to extract heat from a flame zone. Impingement of linear arrays of droplets on the 32 mm cylinder considered earlier will be studied to characterize droplet impingement and secondary breakup on the surface of a cylinder. This cylinder will also be heated to study the effects of a heated surface on droplet vaporization and transport, as a droplet approaches the heated surface. Phase Doppler interferometry and PIV measurements will be carried out to provide the spray and flow field characteristics upstream and downstream of the obstacles. The results will be used to provide data for input and validation for the subgrid turbulence model of the VULCAN fire code.

#### Conclusions

PIV measurements and numerical predictions of a turbulent flow over cylindrical obstacles are presented. Comparisons of the flow field CFD predictions to the measurements show reasonable agreement. A numerical sensitivity study of initial droplet size reveals that droplet penetration around obstacles is dependent on droplet size. Future efforts of this work are to better understand these sensitivities for optimization of liquid suppressant delivery systems on larger-scale experimental platforms.

#### Acknowledgements

The authors wish to acknowledge the partial support of this research by the Department of Defense Next Generation Fire Suppression Technology Program, funded by the DoD Strategic Environmental Research and Development Program. The numerical work was performed in part at Sandia National Laboratories, a multiprogram laboratory operated by Sandia Corporation, a Lockheed-Martin Company, for the U.S. Department of Energy under contract DE-AC04-94AL85000. The authors also wish to thank Dr. G. Papadopoulos of Dantec Dynamics, Inc. for his assistance in recording and post processing the PIV results, and Mr. R. Fink for his assistance in completing the NIST facility modifications.

#### References

1. Widmann, J. F., Charagundla, S. R., Presser, C., and Heckert, A. (1999). "Benchmark Experimental Database for Multiphase Combustion Model Input and Validation: Baseline Case." National Institute of Standards and Technology Internal Report No. 6286.
2. Flowmap<sup>®</sup> 3D-PIV System Owner's Manual, Dantec Measurement Technology, Inc., Mahwah, NJ, July 1999.
3. DesJardin, P.E., Gritzo, L.A., Tieszen, S.R., "Modeling the Effect of Water Spray Suppression on Large-Scale Pool Fires", Proc. Halon Options Technical Working Conference (HOTWC 2000), Albuquerque, NM, May 2-4, 2000.
4. Yang, J.C., Bryant, R.A., Huber, M.L., Pitts, W.M., "Experimental Investigation of Extinguishment of Laminar Diffusion Flames by Thermal Agents," Proc. Halon Options Technical Working Conference (HOTWC 2000), Albuquerque, NM, May 2-4, 2000.

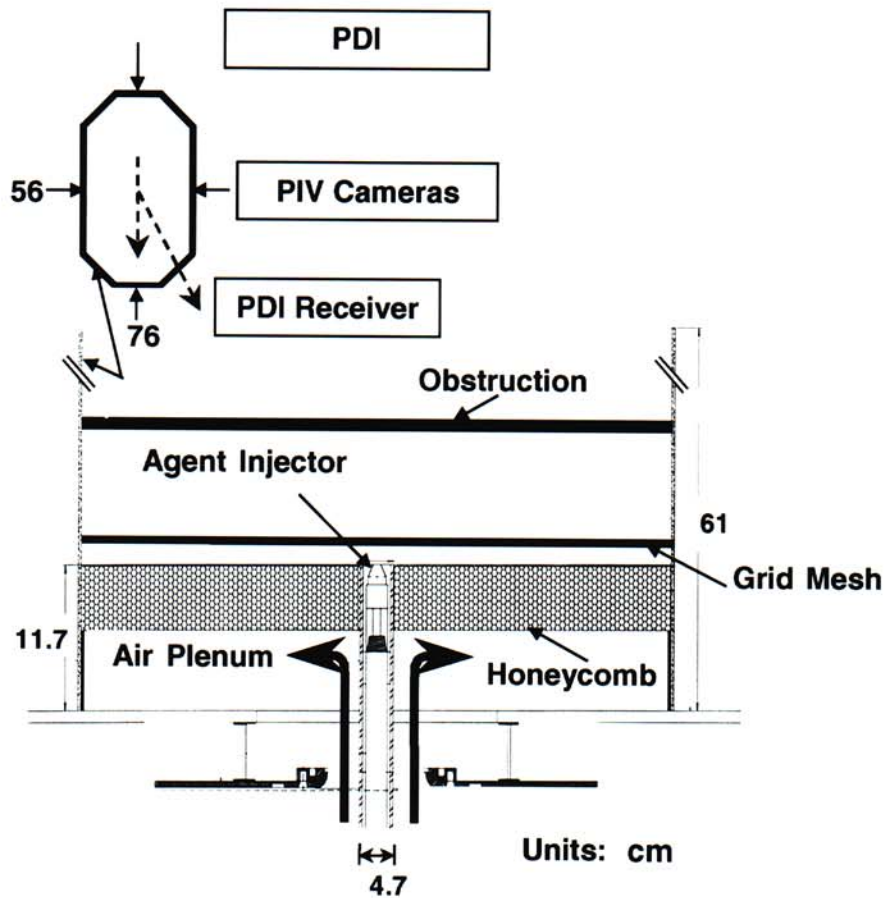


Figure 1: Schematic of the experimental arrangement for mesh-generated air turbulence (not to scale).

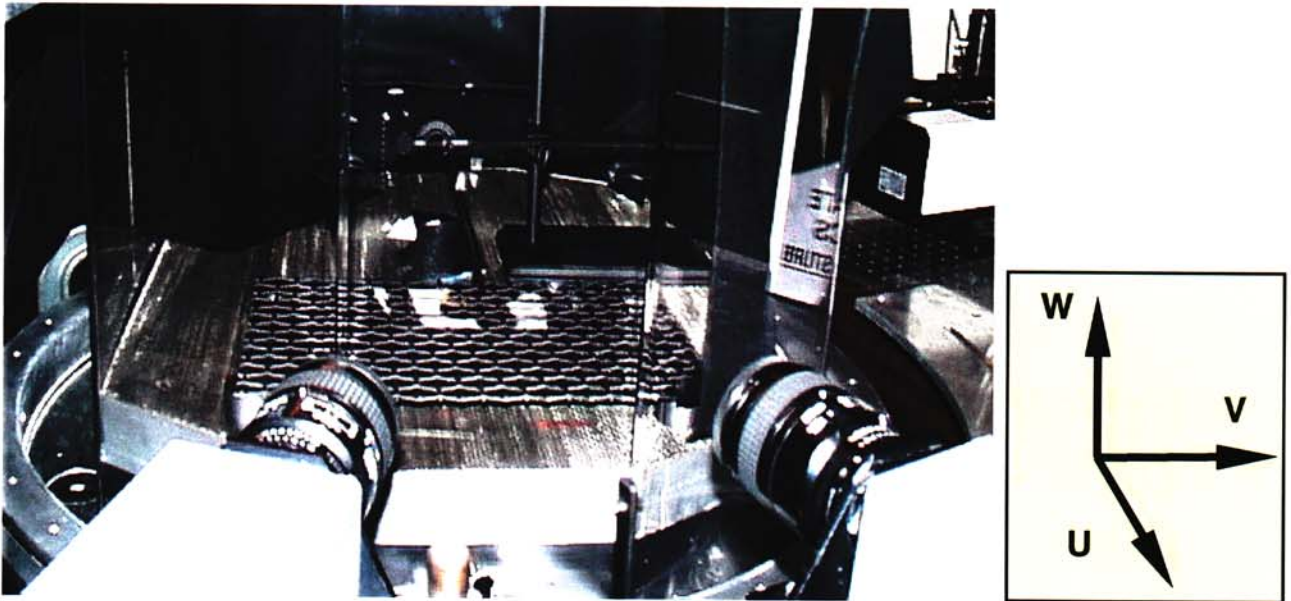


Figure 2: View of the current experimental arrangement with cameras from the PIV system in the foreground.

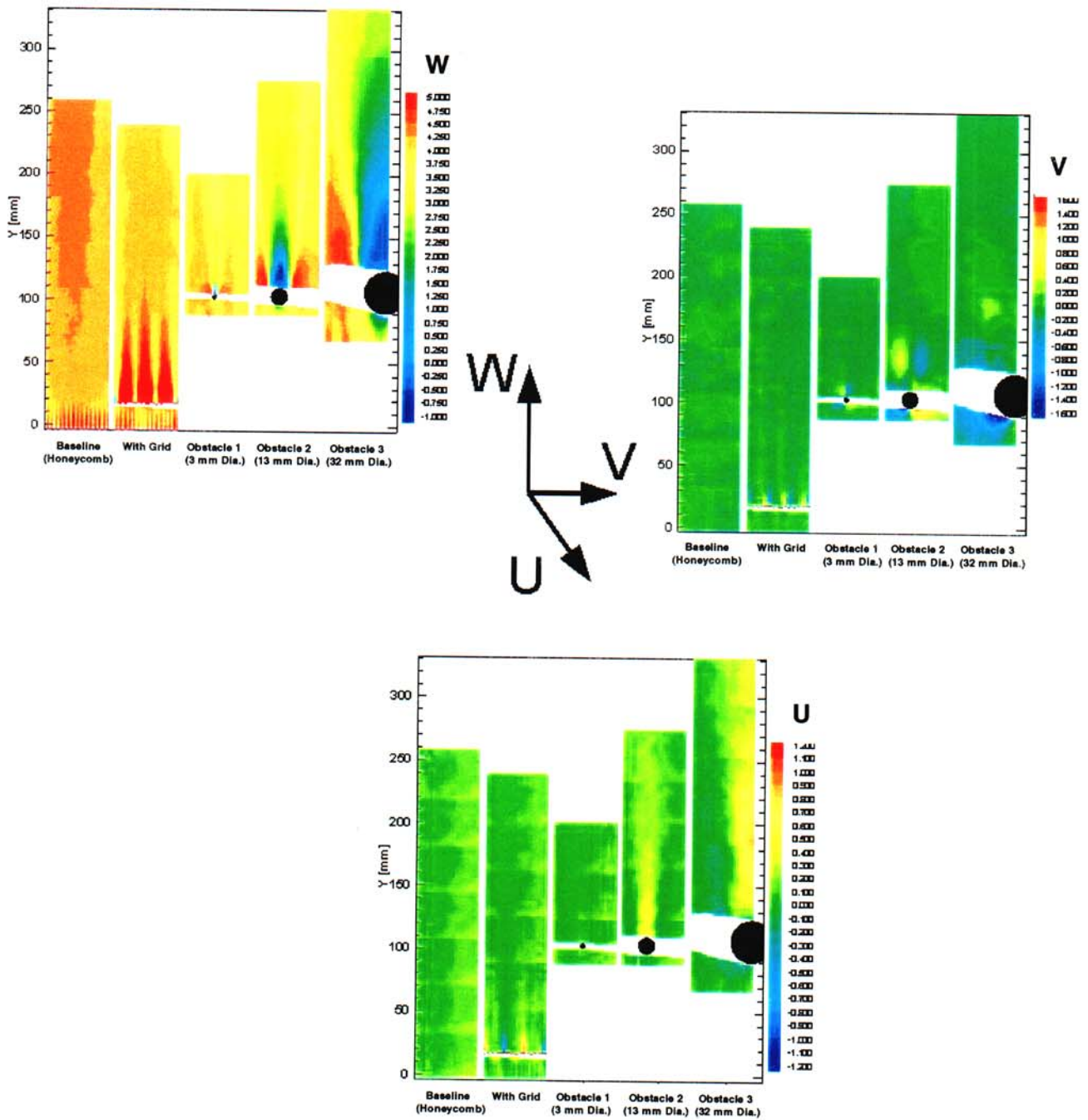


Figure 3: Variation of mean streamwise and cross-stream velocities with downstream distance.

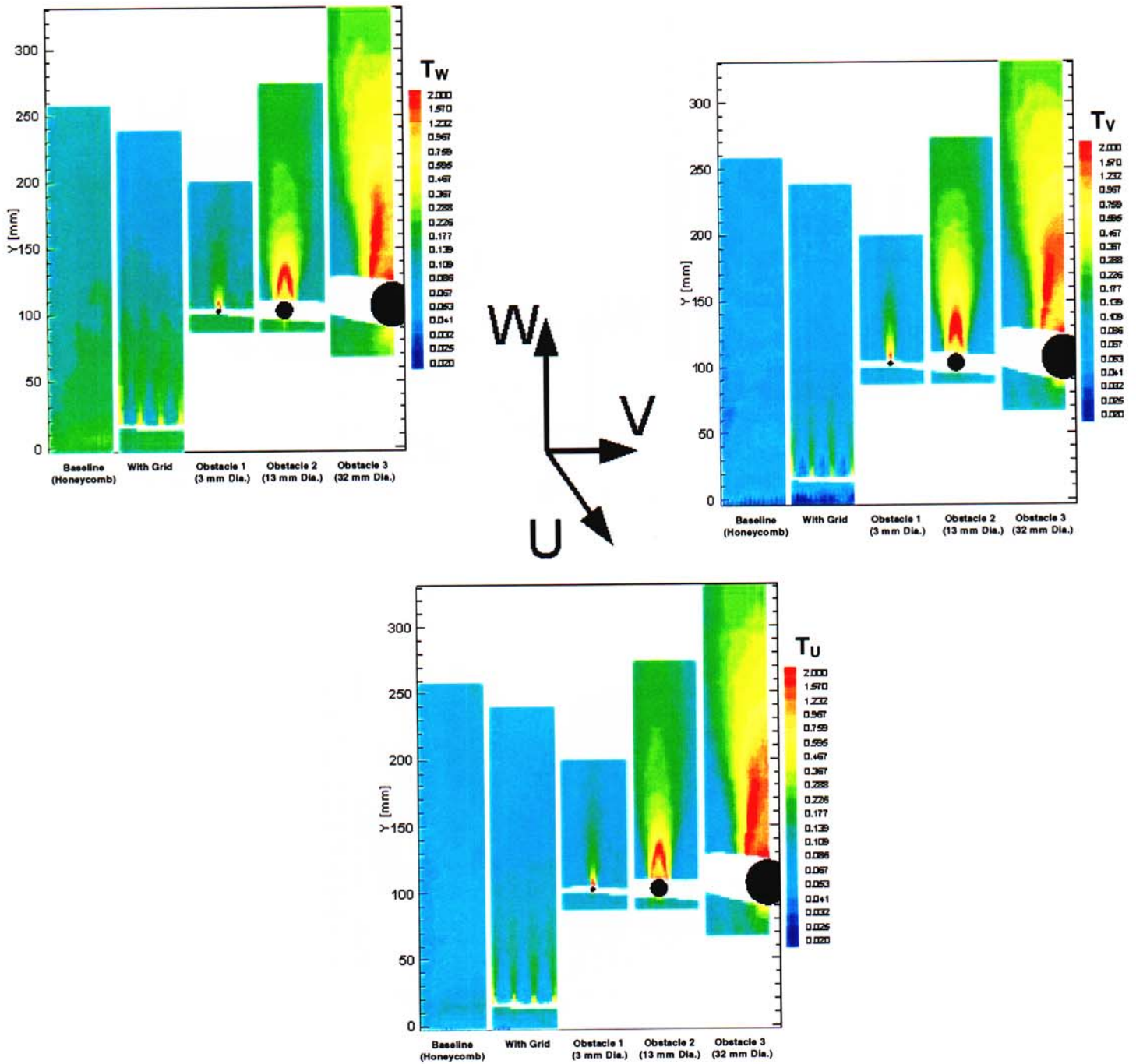


Figure 4: Variation of mean streamwise and cross-stream turbulence intensities with downstream distance.

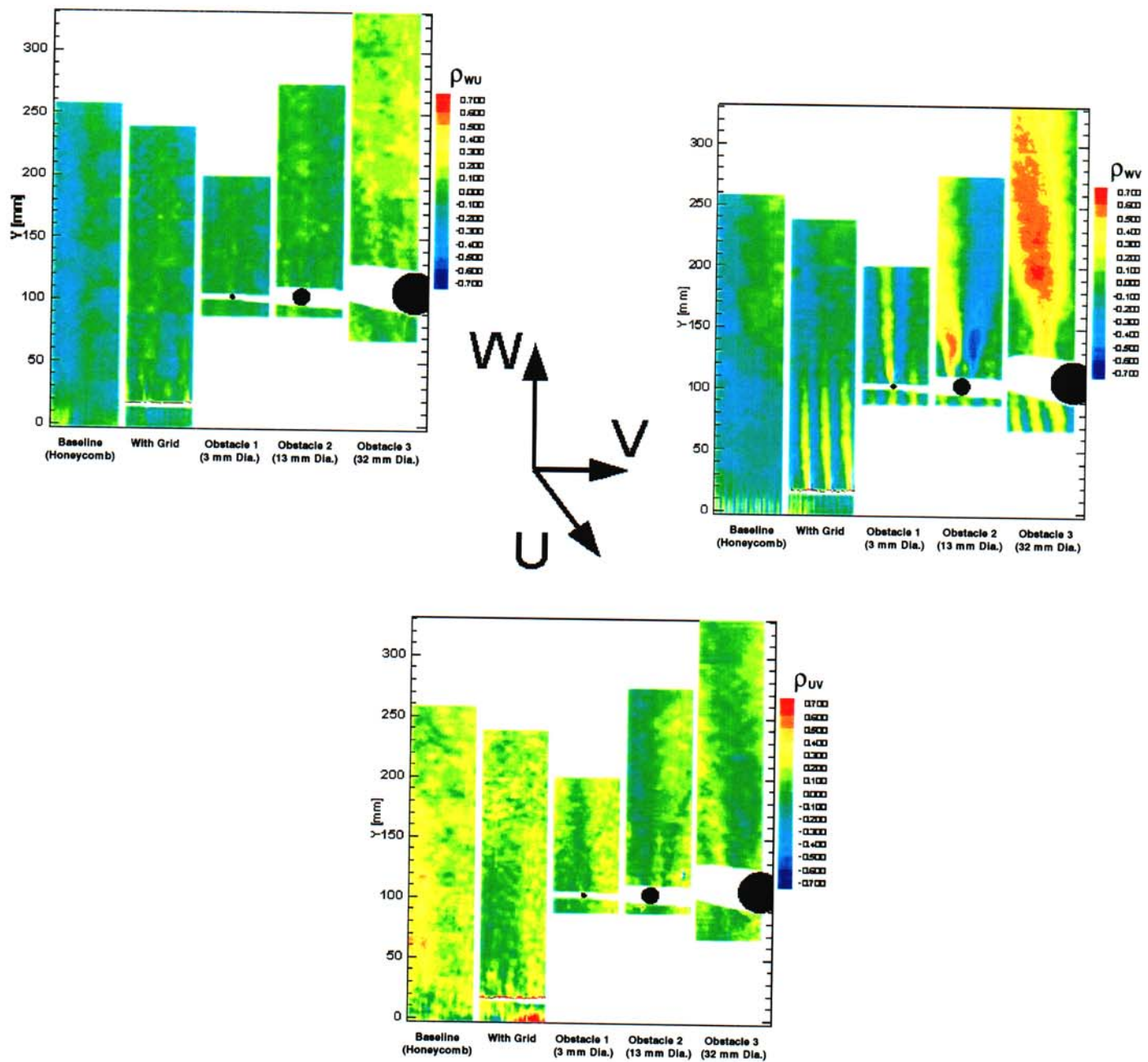


Figure 5: Variation of the correlation coefficients of the turbulent velocity fluctuations with downstream distance.

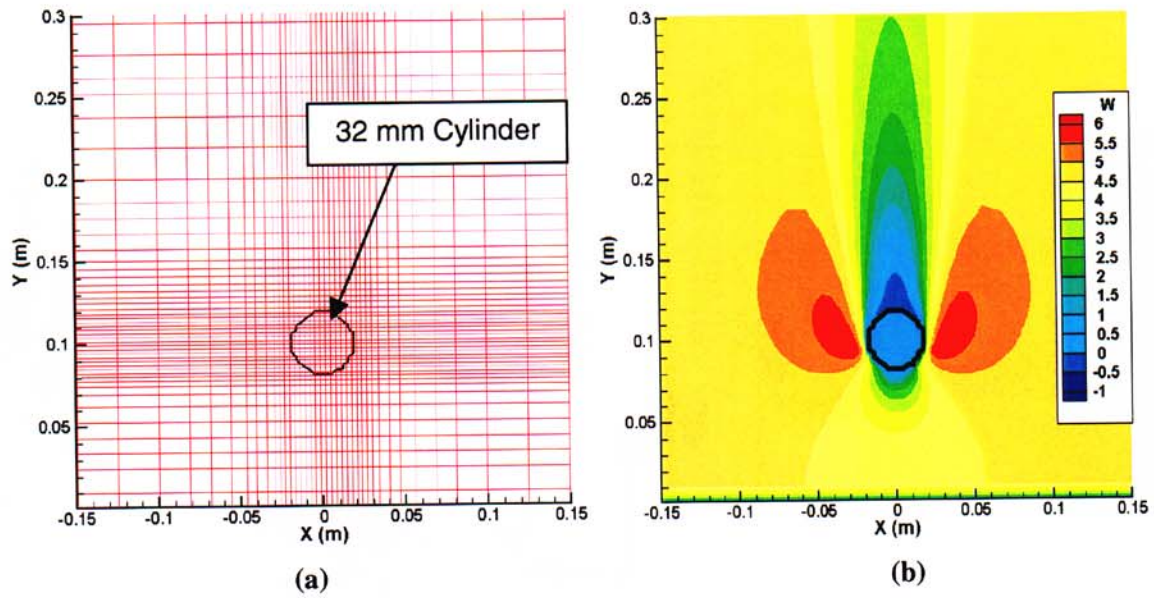


Figure 6: Cross-sectional views of CFD mesh showing (a) mesh refinement around the cylinder and (b) mean streamwise velocity.

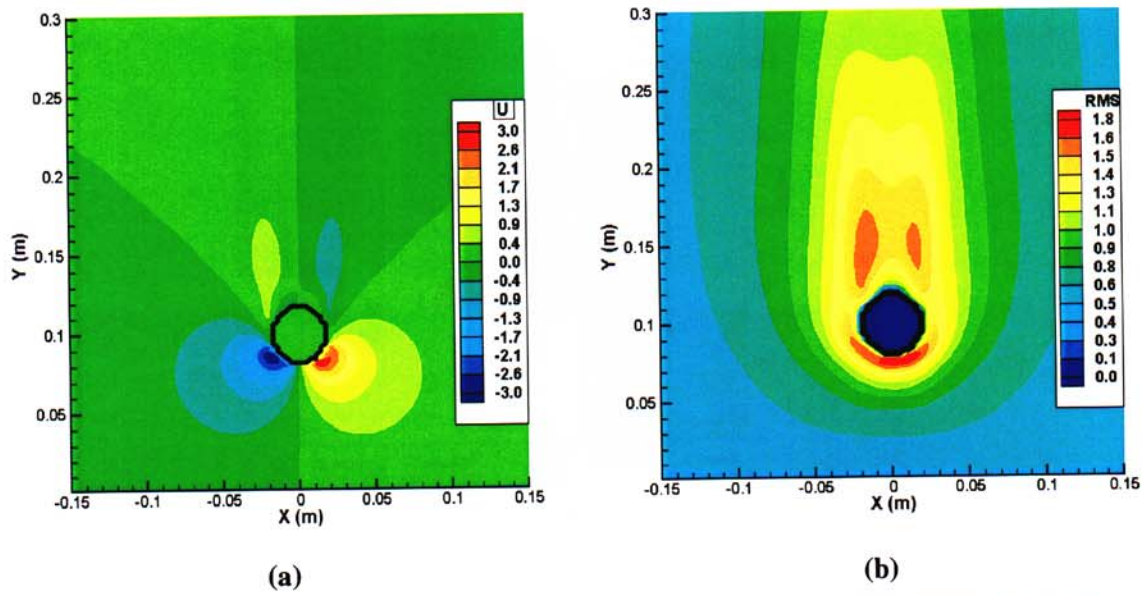


Figure 7: CFD predictions of (a) mean cross-stream velocity and (b) estimate of cross-stream fluctuation.

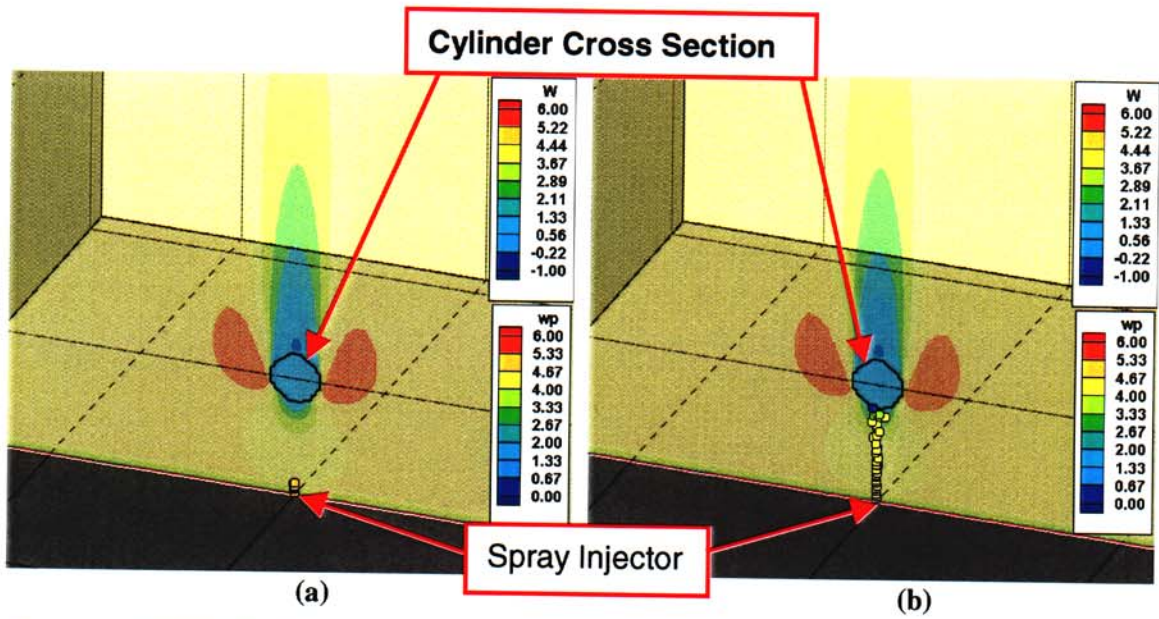


Figure 8: Instantaneous snapshots of the droplet transport around the 32 mm cylinder for (a) 10  $\mu\text{m}$ , and (b) 100  $\mu\text{m}$  droplets.

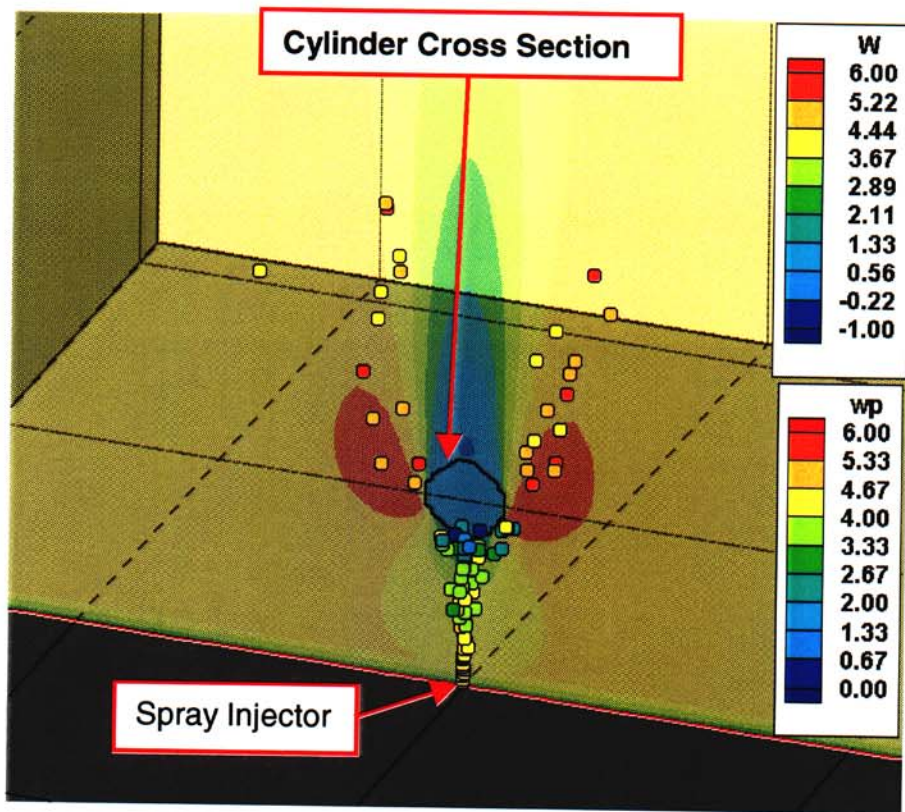


Figure 9: Instantaneous snapshot of the droplet transport around the 32 mm cylinder for 50  $\mu\text{m}$  droplets.